Journal of Nuclear Materials 207 (1993) 116–122
North-Holland

journal of nuclear materials

Impurity transport under steady-state magnetized plasma bombardment in PISCES-B Mod

M.J. Khandagle, Y. Hirooka and R.W. Conn
Institute of Plasma and Fusion Research, University of California at Los Angeles, Los Angeles, CA 90024, USA

J.N. Brooks and A. Hassanein
Argonne National Laboratory, 9700 South Cass Avenue, Argonne, IL 60439, USA

R.B. Turkot, Jr.
Department of Nuclear Engineering, University of Illinois, 103 South Goodwin Avenue, Urbana, IL 61801, USA

Received 10 March 1993; accepted 18 May 1993

Erosion and redeposition of materials is a critical issue in determining the lifetime of plasma-facing components as well as the plasma cleanliness in fusion reactors. In this work, both experimental and modeling efforts have been made to understand the fundamental aspects of the materials erosion and redeposition behavior under plasma bombardment, using the PISCES-B Mod facility, the WBC impurity transport code, and the VFTRIM and ITMC surface codes. A small impurity source made of molybdenum or boron embedded in a host surface of graphite is exposed to a steady-state, magnetically confined argon plasma. The plasma density is about 2×10^{12} cm^{-3}, and the electron temperature is about 18 eV. The ion bombarding energy to the surface is set at 100 and 150 eV. The magnetic field is about 500 G. Under these experimental conditions, about 70% of the sputtered impurity atoms are calculated to be redeposited on the graphite surface, resulting in a distribution of impurity atom concentration on the graphite surface. The measured impurity redeposition profile indicates a decay across the magnetic field, and reaches a steady-state profile after a certain plasma exposure time. A good agreement has been found between the experimental data and the results of modeling.

1. Introduction

In magnetic fusion devices, materials eroded from the plasma-facing components can be ionized due to electron impact, trapped by the magnetic field and then redeposited elsewhere. The materials transport associated with erosion and redeposition can affect the lifetime of plasma-facing components and has a direct impact on the plasma cleanliness.

To understand the edge impurity transport and material redeposition, several experiments have been performed in tokamaks such as the Tokamak Fusion Test Reactor (TFTR) [1] and the Doublet III-D (DIII-D) [2] during extended campaigns consisting of many tokamak discharges of a few second duration. Generally, data on the archaeology of impurity redeposition can be obtained only during vacuum openings. It is also true that such archaeological analysis of the impurity transport may be significantly affected by off-normal events such as disruptions and run-away electrons. A number of single pulse erosion/redeposition measurements are being planned for DIII-D using the Divertor Materials Evaluation System (the DIMES probe) [3]. However, these are limited in number and duration due to tokamak operation constraints.

One finds, therefore, an important role that non-tokamak, steady-state plasma devices can play in understanding the details of materials transport associated with erosion and redeposition processes. Using the Plasma Interaction with Surfaces and Components Experimental Station, PISCES-A facility, the first non-tokamak experiments on materials redeposition were carried out for selected materials under controlled conditions [4]. In this work simple analysis was

performed to explain the net erosion data under redeposition conditions. Due to the incompleteness of plasma diagnostics on PISCES-A and the lack of modeling capability, it was not possible to analyze the details of materials transport associated with redeposition.

In the present work, the PISCES-B Mod facility [5,6] is used to study these details under well-diagnosed experimental conditions. The redeposition-driven cross-field transport behavior of selected impurities (boron and molybdenum) over a graphite target has been investigated under argon plasma bombardment with a normal incidence of the magnetic field. The WBC code [7] is used to model the impurity transport in these experiments with the help of the Vectorized Fractal TRIM (VFTRIM) code [9,10] which provides information on the velocity distribution of sputtered atoms. The effective erosion yield of the molybdenum marker contaminated by redeposited impurities is calculated using the Ion Transport in Materials and Compounds (ITMC) code [11].

2. Experimental

In PISCES-B Mod, high-density, steady-state cylindrical plasmas of argon, nitrogen, hydrogen, deuterium and helium can be generated in a linear magnetic field that is parallel to the main axis of the vacuum chamber. Shown in fig. 1a is a schematic diagram of the present experimental setup. An "impurity" marker made of molybdenum or boron is embedded in the center of a graphite target circular plate with a diameter of 5 cm. The target is exposed to a steady-state argon plasma for a total time duration of about one hour. The effective ion bombarding energy is controlled by applying a negative dc-bias on the graphite target. Two effective ion bombarding energies of 100 eV and 150 eV are used in these experiments: one is below the calculated threshold energy for physical sputtering of graphite by argon [8] and the other is above the threshold. The target is positioned normal to the plasma axis and the axial magnetic field is set at about 500 G. Under these conditions, material sputtered from the impurity marker can be ionized in the plasma and has a relatively high probability of redeposition on the graphite surface, as will be described later. Shown in fig. 1b is an example of the trajectory of a sputtered atom modeled by the WBC code, details of which will be described in section 3.2.

A fast-acting pneumatic double probe [6] is used to measure the radial profile of the plasma density and electron temperature near the substrate surface. The radial plasma density and space potential profiles are

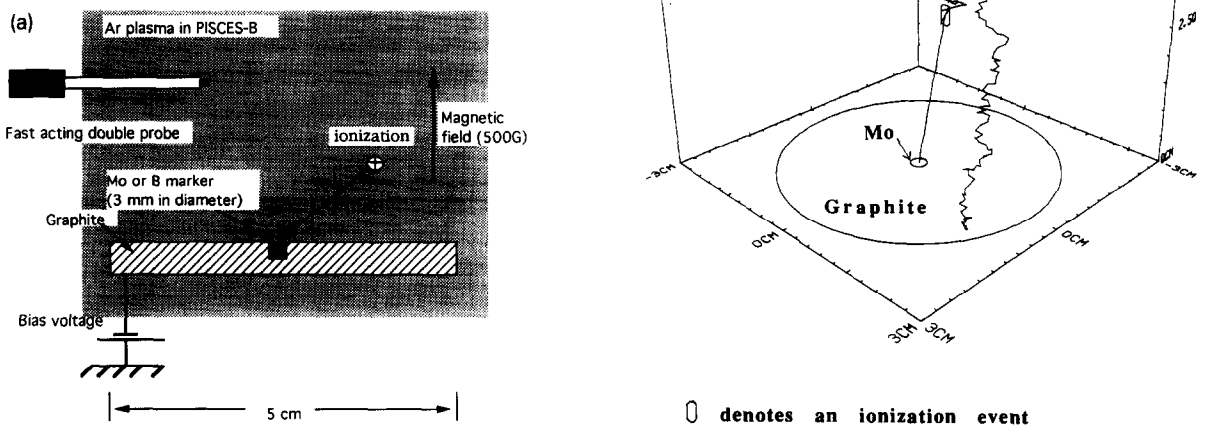

Fig. 1. (a) A schematic diagram of the experimental setup. (b) A particle trajectory calculated with the WBC Monte Carlo code [7], showing the sputtering and redeposition paths of a Mo atom.

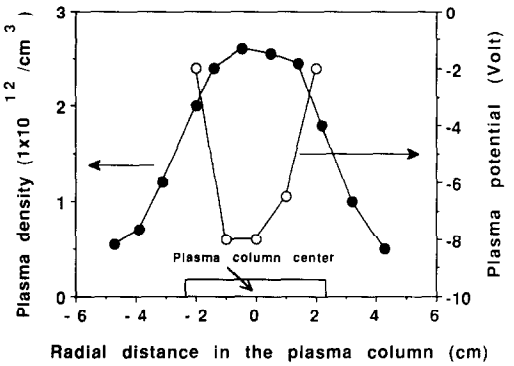

Fig. 2. Typical argon plasma density and potential profiles in PISCES-B Mod.

shown in fig. 2. The plasma density over the target area is maintained at about 2×10^{12} cm^{-3} and the electron temperature is set at about 18 eV. The ion bombarding flux is about 1×10^{18} ions/cm^2 s. The space potential profile is measured across the plasma column. Data indicate a radial electrostatic field such that the center of the plasma is at a lower potential than the edge. Under these conditions, the radial velocity component of impurity ions will be reduced, leading to an improvement of ion confinement. Therefore, this electrostatic field enhances the redeposition of ionized impurities. In order to analyze the time evolution behavior of impurity transport, the plasma exposure time is increased in steps up to a total exposure of one hour.

After plasma exposure, surface analysis is performed to obtain the impurity distribution profile. Since the Mo marker is at the center of the circular graphite target, for a given radial distance from the center of the Mo marker the concentration of redeposited Mo over the graphite surface is expected to have a azimuthal symmetry. Hence the radial Mo concentration profile is obtained by measuring the Mo concentration along a single radius of the graphite substrate. Energy-dispersive X-ray analysis (EDX) and Auger electron spectroscopy (AES) are used to determine the surface impurity concentration. The depth of analysis with EDX is about 50 nm for Mo and 150 nm for carbon. EDX analysis has a high sensitivity to Mo. Hence, the radial impurity concentration profile after each plasma exposure is obtained by EDX. Quantitative analysis is performed using pure element standards as references. The error in this analysis ranges from 2% at the high concentrations (≥ 1 at%) to 20% at low concentrations (≤ 0.1 at%) measured. The depth of analysis with AES is a few nm. The error in AES quantitative analysis is about 5%.

3. Results and discussion

3.1. PISCES experiments

The Mo radial concentration profiles from EDX analysis are shown in fig. 3. During EDX analysis no carbon contamination was detected at the Mo marker even after 60 min exposure. Hence in fig. 3, the Mo concentration is shown to be 100 at% on the marker surface. The Mo concentration on the graphite surface is observed to decrease with increasing radial distance. As shown in fig. 4, the Mo concentration at several radial positions along a single radius on the graphite surface changes as a function of time in such a way that

$$C = C_0[1 - \exp(-t/\tau)],$$

where C is the Mo concentration, τ is the characteristic time constant and C_0 is the steady-state concentration. The calculated values of the characteristic time constants are shown in table 1. Notice that the calculated time constants at 100 eV are significantly higher than those at 150 eV. The Mo steady-state concentrations at 100 eV energy are higher than at 150 eV. In

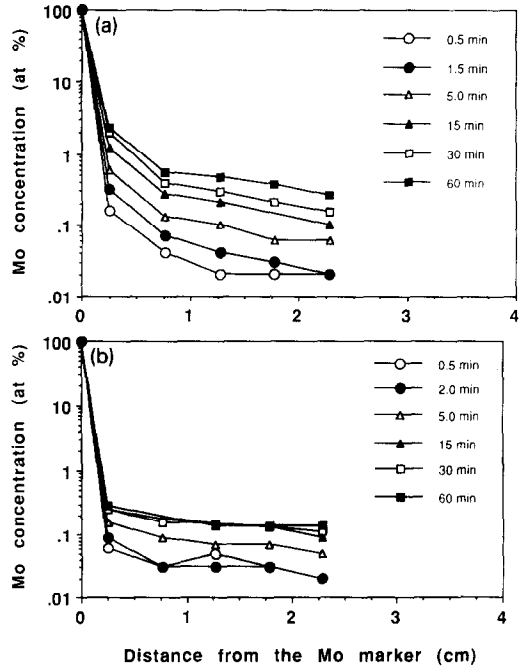

Fig. 3. Radial concentration profiles of Mo redeposited on the graphite target obtained by EDX analysis along a fixed radius. The target was bombarded with (a) 100 eV Ar^+ ions, (b) 150 eV Ar^+ ions.

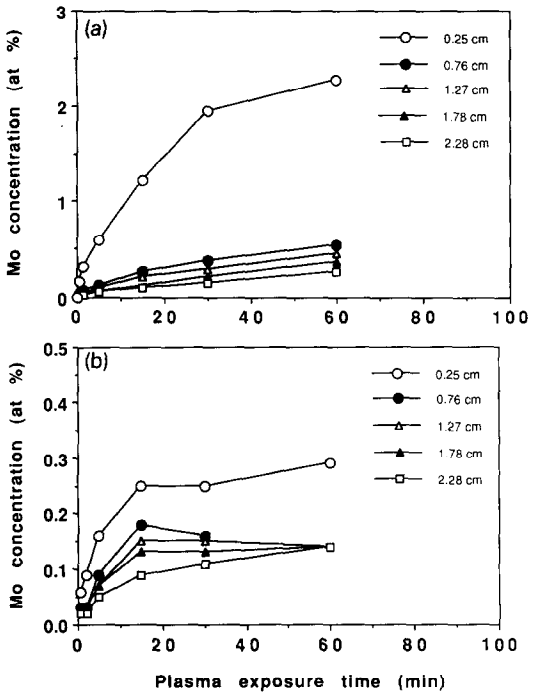

Fig. 4. Time evolution of Mo concentration at different radial positions along a fixed radius on the graphite surface. The target was bombarded with (a) 100 eV Ar^+ ions, (b) 150 eV Ar^+ ions. The numbers in the legend indicate the distance from the center of the marker.

general, the time dependence of Mo concentration on the graphite surface at a given radial position is expected to be determined by the respective sputtering rates of Mo at the marker and in the carbon, and by the transport of the sputtered Mo. The observed behavior is found to be consistent assuming that redeposited carbon atoms gradually cover up the marker, thereby reducing Mo erosion. To confirm this point, in-situ AES was performed. AES is more sensitive to the presence of carbon on Mo than EDX because, the Mo has a very high absorption coefficient for carbon X-rays generated during EDX analysis. AES data indicates that the Mo marker surface is indeed covered with redeposited carbon to a concentration of 23 at% after a 60 min exposure at 150 eV energy, and to a concentration of 16 at% at 100 eV. Possible effects of the carbon coverage over molybdenum are discussed in section 3.3.

Table 1
Characteristic time constants for Mo concentration buildup

Impurity marker material	Argon bombarding energy (eV)	Radial position from the center (cm)	Characteristic time constant, τ (min)
Mo	100	0.25	16
		0.75	25
		1.25	29
		1.75	40
		2.25	36
Mo	150	0.25	8.3
		0.75	5.8
		1.25	7.2
		1.75	4.6

The transport of boron has also been studied under identical experimental conditions. Generally, trends similar to molybdenum have been found for boron. The only difference observed is that the steady-state profile for boron was established much more rapidly than that for molybdenum. In fact, the characteristic time constant for boron is typically about a few minutes. This appears to be due to the fact that the sputtering yield of boron is generally high, providing a strong intensity impurity source.

3.2. WBC simulation of impurity redeposition

Impurity redeposition under the PISCES-B Mod conditions has been simulated using the WBC Monte Carlo code [7]. WBC is a 3-D kinetic code which computes the subgyro orbit motion and the charge state of sputtered impurities in a fixed background plasma. It contains models for sputtering, electron impact ionization and recombination (and other relevant atomic and molecular processes), velocity changing collisions with the plasma, and sheath parameters. In the code, a sputtered neutral is launched from the surface with velocity determined by a sputtering subcode, or in some cases by an analytic model. The point of neutral ionization is then determined based on the locally-varying electron density and temperature. Once ionized, the particle velocity is computed based on the Lorentz force motion plus impurity–plasma collisions. Collisions are computed via a Monte Carlo solution of the Fokker–Plank equations, which as discussed in ref. [7], involve terms for collisional friction of the impurities with the background plasma, and velocity diffusion. The ion charge state is computed simultaneously, via a standard Monte Carlo method. The simulation is performed using the plasma parameters obtained from measurements done in PISCES-B Mod:

(1) Argon plasma with an ion temperature of 0.2 eV.
(2) Plasma density and electron temperature profiles corresponding to the measured values.
(3) A Debye-type sheath region with a negative bias of 100 or 150 V.
(4) A presheath electric field of about 30 V/m.
(5) A radial electric field corresponding to a parabolic potential difference with a measured value of $\Delta\Phi = 6$ V at a radius of $r = 3$ cm (see fig. 2).
(6) Bohm diffusion for radial transport.

The sputtering process is modeled by the vectorized fractal TRIM (VFTRIM) code [9,10] to provide the velocity distribution of sputtered neutral atoms to the WBC code. In the VFTRIM code the effect of surface roughness on ion–surface interactions is handled using the fractal concept. For comparison, a cosine angular distribution and a Thompson energy distribution having a maximum cut-off energy for the sputtered atoms is also used as an input to the WBC code. It was found that the VFTRIM-based simulations show a considerably better agreement with the experimental data, as will be shown later.

The WBC code computes the charge state of an ion due to electron impact ionization (recombination being negligible here) as a function of time. Approximately 10000 particles are launched (corresponding to about 70000 incident Ar^+ ions at 100 eV), from the 3 mm diameter marker (for Mo and B), or from the 5 cm diameter substrate (graphite) for each simulation. A particle history terminates upon the particle's reaching anywhere on the surface, or upon its leaving the plasma column in PISCES-B Mod.

WBC runs were made for Mo and B transport and also for carbon transport. In the latter case carbon is sputtered uniformly from the entire carbon surface. Fig. 1b shows an example of a sputtered particle trajectory. As shown, the particle is sputtered as a neutral atom which has a straight line trajectory until it is ionized. Once ionized, due to the presence of magnetic and electrostatic fields, the particle undergoes a complex motion dependent upon its radial diffusion, thermalizing collisions with the plasma, gyro motion, and its changing charge state. In the case shown in fig. 1b, the particle is redeposited on the target. Table 2 summarizes the results of the WBC simulations. The WBC results show the following trends: the elevation angle, $\bar{\Theta}$, measured from the normal to the surface is only a few degrees and indicates that redeposited ions of B as well as Mo impact the graphite surface at essentially normal incidence, with energy, $\bar{E}$, determined primarily by their acceleration through the sheath due to the dc-bias applied. The Mo ions reach a higher charge state, $\bar{K}$, than the B ions. The spatially averaged redeposition fraction, f, is somewhat higher for Mo than that for B. This is primarily due to the increased radial confinement of the Mo ions as a result of their attaining higher charge states.

Table 2
Results of WBC analysis of the PISCES Mo and B transport experiments. An overbar denotes average value. All parameters except the first two refer to redeposited particles. The plasma parameters used are: $T_e = 20$ eV, $N_e = 2\times10^{12}$ cm^{-3} for molybdenum and carbon redeposition and $T_e = 17$ eV, $N_e = 2.5\times10^{12}$ cm^{-3} for boron

Parameter	Mo	Mo	B	C
Incident Ar^+ ion energy (eV)	100	150	100	150
Sputtered particle energy, $\bar{U}_0$ (eV)	4.4	5.9	2.4	4.4
Redeposition fraction, f	0.76	0.72	0.65	0.42
Ion transit time, $\bar{t}$ (μs)	19	20	7	11
Elevation angle, ($\bar{\Theta}$) (degrees)	4	3	2	3
Charge state, $\bar{K}$	2.3	2.4	1.0	1.1
Energy of redepositing ions, $\bar{E}$ (eV)	240	368	103	170

Normalized Mo concentration profile data at the exposure period of 0.5 min is compared with the WBC simulated redeposition flux profile in fig. 5. Here, normalization is done using the data at a position 0.25

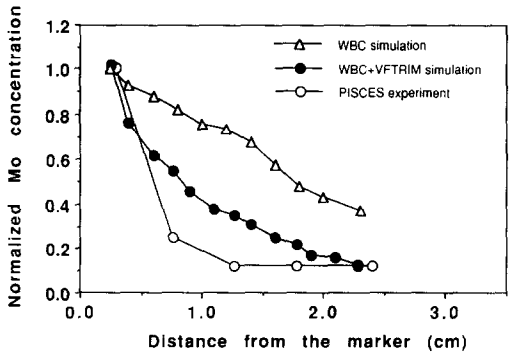

Fig. 5. Comparison of molybdenum redeposition data from the PISCES experiments with those from the WBC simulation. The total exposure time is set at 0.5 min for this comparison to avoid the time accumulation effect.

cm from the center because in the case of the PISCES experiments, the redeposition of Mo on the marker surface cannot be differentiated from the marker material. Considering that there is a factor of two uncertainty in the measurement of the plasma parameters and in the ionization rate coefficient data used as input to the WBC code, the WBC profile with the VFTRIM input agrees quite well with the experimentally observed trend of decrease in Mo concentration with increase in the distance from the marker.

In the case of the experiments performed in PISCES, the impurity concentration on the graphite surface increases with increasing time and tends to reach a steady state value as described earlier. The Mo redeposited on the graphite acts as a secondary source of impurity and can be expected to influence the measured redeposition profile. The WBC code cannot take into consideration changes in marker size or purity with time. We discuss the issue of sputtering of Mo deposited on graphite in the next section. In our comparison of the WBC results we have used the PISCES data for the smallest exposure period of 0.5 min to minimize the effect of a change in the impurity source. Also, we have normalized and compared data obtained for all the exposures up to one hour and there is no difference between the normalized Mo concentration profiles for the smallest or the longest exposures. Therefore, we can assume that the nature of the normalized profile does not change appreciably with time and that the comparison shown in fig. 5 is valid.

3.3. Mo impurity concentration on graphite

In this section, we attempt to explain the observed time evolution of the Mo redeposition behavior. The net Mo atom flux on the graphite substrate is related to the difference between the redeposited flux of Mo sputtered from the marker and the flux of Mo atoms eroded from the graphite substrate after redeposition. The flux of redeposited Mo atoms is proportional to the flux of Mo sputtered off the marker surface (the redeposition fraction is calculated from the WBC code to be around 75%). The Mo sputtering from the marker surface, however, is sensitive to the surface contamination. As mentioned earlier, from in-situ AES analysis performed after 60 min plasma exposure, we have found evidence of 16 and 23 at% of carbon deposited on the marker surface in the case of 100 and 150 eV Ar^+ bombardment, respectively. A partial surface coverage of the Mo marker with carbon redeposited from the graphite surface can substantially reduce the sputtering yield of molybdenum due to a screening effect [12]. In order to analyze this screening effect, we have run the ITMC code.

The ITMC code [11] is a 3-D Monte Carlo code which computes ion penetration and sputtering in target materials. The sputtering yields of single element targets as well as alloys with different surface and bulk compositions, or of layered structures of different materials can be simulated. The layer thickness can be as small as a monolayer. The code computes incident particle and recoil particle trajectories based on a binary nuclear collision model. A variety of energy loss models are used in the code as appropriate for the surface composition in question. For each species, the individual contribution of primary and secondary knock-on atom cascades to the total sputtering yield is also evaluated.

The ITMC results for 100 eV Ar^+ ions incident on a (Mo + C) homogeneous mixture are shown in fig. 6a as a function of Mo concentration. The effect of an increase in thickness of the surface layer of carbon on molybdenum is shown in fig. 6b. It is clear from fig. 6a

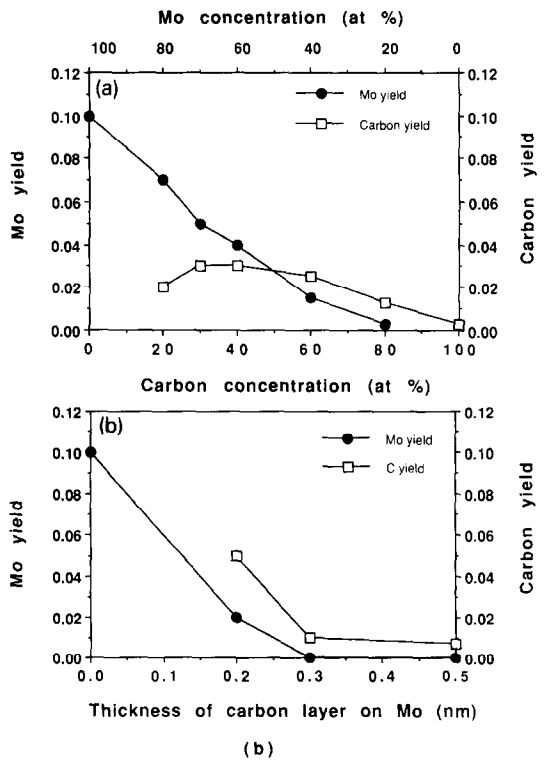

Fig. 6. Sputtering yield calculated with the ITMC code for (a) Mo and carbon homogenous mixture, (b) Mo covered with carbon up to a few monolayers.

that even a slight increase in Mo concentration can increase the carbon sputtering yield noticeably. This is mainly because of the near-surface collisional cascade effects of Mo atoms. Thus, as the Mo concentration on the graphite surface increases, the sputtering rate of graphite increases. Also, in the case of an homogenous mixture of (Mo + C) the erosion yield of Mo reduces linearly as the carbon concentration increases. In the case of the carbon layer coverage shown in fig. 6b, the erosion yield of Mo reduces by a factor of 5 for a 0.2 nm thickness of carbon layer and is indicative of a complete suppression when the carbon layer thickness is above 0.3 nm. This occurs because when the Mo marker is covered by carbon, the contribution of the primary knock-on cascades to the sputtering of Mo is substantially reduced, and the energy transfer from secondary cascades of the light carbon atoms is poor.

In summary, the observed time evolution of Mo transport can be qualitatively explained as follows: as the Mo impurity concentration increases on the graphite surface, the effective sputtering yield of carbon increases and hence carbon redeposition on the Mo marker increases. The increase in carbon redeposition on the marker in turn contributes to a decrease in the Mo flux sputtered from the marker and redeposited on the graphite. At some point the fluxes of redeposited Mo to the graphite surface and Mo eroded from the graphite surface balance each other, which leads to the steady state Mo concentration. More elaborate analysis using a fully coupled WBC/ITMC calculation can be done for the time-dependent impurity transport, but this is beyond the scope of the present work.

4. Summary

With the main emphasis of understanding the fundamental processes of impurity transport, materials redeposition experiments have been carried out in PISCES-B Mod. The effect of redeposition due to the cross-field impurity transport has been clearly demonstrated in these experiments. It is also found that as plasma exposure proceeds, the impurity concentration profile exhibits a breakthrough time evolution with an exponential increase followed by a steady-state behavior. These experimental data have been analyzed using the WBC impurity transport code. The experimentally observed decreasing trend for the Mo concentration with increasing distance from the marker is predicted quite well by the WBC code. Considering that there is a factor of two uncertainty in the plasma parameters and the ionization rate coefficients we believe that the agreement between the experimental data and the WBC code results with VFTRIM input is good. Also, using the effective sputtering yield calculated by the ITMC code, the experimentally observed steady state is qualitatively explained.

Acknowledgements

The work performed at the PISCES laboratory is supported by the US Department of Energy under contract DE-FG03-86ER-52134. R.B. Turkot, Jr. is supported by the Magnetic Fusion Energy Technology Fellowship. We also wish to thank Y. Ra (LAM Research Corporation) and D.N. Ruzic (University of Illinois) for their useful suggestions.

References

[1] R.T. McGrath and J.N. Brooks, J. Nucl. Mater. 162–164 (1989) 350.
[2] B.E. Mills, D.N. Hill, J.P. Smith, W.L. Hsu and A.E. Pontau, J. Nucl. Mater. 176&177 (1990) 947.
[3] C.P.C. Wong et al., J. Nucl. Mater. 196–198 (1992) 871.
[4] Y. Hirooka et al., J. Nucl. Mater. 141–143 (1986) 193.
[5] Y. Hirooka et al., J. Vac. Sci. Technol. A8 (1990) 1790.
[6] Y. Hirooka, ed., PISCES Program, Progress Report for 1990–1991 on Plasma–Materials Interactions and Edge–Plasma Physics Research, UCLA Report #PPG-1380 (1991).
[7] J.N. Brooks, Phys. Fluids B2(8) (1990) 1858.
[8] Y. Yamamura, N. Matsunami and N. Itoh, Radiat. Eff. 71, (1983) 65.
[9] D.N. Ruzic, Nucl. Instr. and Meth. B47 (1990) 118.
[10] M.A. Shaheen, A Fractal Surface Model for Multi-Component TRIM: Applications to Boron–Carbon Materials, M.S. Thesis, Department of Nuclear Engineering, University of Illinois, 1992.
[11] A. Hassanein and D. Smith, Nucl. Instr. and Meth. B13 (1986) 225.
[12] K. Morita, Fusion Technol. 19 (1991) 2083.